J|A|C|S
ARTICLES
Published on Web 12/29/2006

Following Photoinduced Dynamics in Bacteriorhodopsin with 7-fs Impulsive Vibrational Spectroscopy

Anat Kahan,† Omer Nahmias,† Noga Friedman,‡ Mordechai Sheves,*,‡ and Sanford Ruhman*,†

Contribution from the Department of Physical Chemistry and the Farkas Center for Light Induced Processes, Hebrew University, Jerusalem 91904, Israel, and Department of Organic Chemistry, The Weizmann Institute of Science, Rehovot 76100, Israel

Received July 11, 2006; E-mail: mudi.sheves@weizmann.ac.il; sandy@fh.huji.ac.il

Abstract: Sub-10-fs laser pulses are used to impulsively photoexcite bacteriorhodopsin (BR) suspensions and probe the evolution of the resulting vibrational wave packets. Fourier analysis of the spectral modulations induced by transform-limited as well as linearly chirped excitation pulses allows the delineation of excited- and ground-state contributions to the data. On the basis of amplitude and phase variations of the modulations as a function of the dispersed probe wavelength, periodic modulations in absorption above 540 nm are assigned to ground-state vibrational coherences induced by resonance impulsive Raman spectral activity (RISRS). Probing at wavelengths below 540 nm—the red edge of the intense excited-state absorption band—uncovers new vibrational features which are accordingly assigned to wave packet motions along bound coordinates on the short-lived reactive electronic surface. They consist of high- and low-frequency shoulders adjacent to the strong C=C stretching and methyl rock modes, respectively, which have ground-state frequencies of 1008 and 1530 cm^{-1}. Brief activity centered at ~900 cm^{-1}, which is characteristic of ground-state HOOP modes, and strong modulations in the torsional frequency range appear as well. Possible assignments of the bands and their implication to photoinduced reaction dynamics in BR are discussed. Reasons for the absence of similar signatures in the pump−probe spectral modulations at longer probing wavelengths are considered as well.

Introduction

Bacteriorhodopsin (BR) is a membranal proton pump which utilizes solar light to set up a pH gradient across the cellular membrane of *Halobacterium salinarum*. The resulting chemical potential is used to energize its life cycle under extreme environmental conditions.[1−3] The protein is composed of seven transmembrane helices enclosing the binding pocket for an *all-trans* retinal chromophore, which is bound covalently to Lys 216 via a protonated Schiff base (PSB) linkage. Absorption of a photon by the retinal eventually induces isomerization around the C_{13}=C_{14} double bond, initiating a photocycle with several distinct spectroscopic intermediates. Protonation of the Schiff base nitrogen and interactions with the protein shift the retinal absorption from the near-UV to the center of the solar spectrum (λ_{max} = 568 nm), giving the membrane its characteristic purple color.[4] Photon absorption unleashes dramatic subpicosecond spectral changes in BR, consisting of the appearance of a near-IR (NIR) stimulated emission band peaking at ~850 nm and a strong blue absorption around 460 nm, both assigned to the reactive excited state denoted "I_{460}". These features decay within ~1 ps, leading to a longer lived intermediate called "J_{625}", exhibiting a red-shifted peak absorption at 625 nm,[5−14] often assigned as a ground-state species in which retinal is isomerized to a 13-cis configuration. This result is achieved with a quantum efficiency of ~60%,[15,16] making the differentiation of reactive and nonreactive spectral signatures a constant concern when interpreting ultrafast spectroscopic data on BR. The rapid internal conversion and isomerization of BR's retinal prosthetic group is believed to hold the key for the efficient storage of the absorbed photon energy. Constructing a detailed multidimen-

† Hebrew University.
‡ The Weizmann Institute of Science.

(1) Ottolenghi, M., Sheves, M., Eds. *Isr. J. Chem.* **1995**, *35*.
(2) Lanyi, J., Ed. *Biochim. Biophys. Acta Bioenerg.* **2000**, *1460*.
(3) Haupt, U.; Tittor, J.; Oesterhelt, D. *Annu. Rev. Biophys. Biomol. Struct.* **1999**, *21*, 367.
(4) Oesterhelt, D.; Stoeckenius, W. *Nature New Biol.* **1971**, *233*, 149.
(5) Sharkov, A. V.; Pakulev, A. V.; Chekalin, S. V.; Matveets, U. V. A. *Biochim. Biophys. Acta* **1985**, *808*, 94.
(6) Petrich, J. W.; Breton, J.; Martin, J. L.; Antonetti, A. *Chem. Phys. Lett.* **1987**, *137*, 369.
(7) Dobler, J.; Zinth, W.; Kaiser, K.; Oesterhelt, D. *Chem. Phys.* **1988**, *144*, 215.
(8) Kobayashi, T.; Kim, M.; Taiji, M.; Iwasa, T.; Nakagawa, M.; Tsuda, M. *J. Phys. Chem. B* **1998**, *102*, 272.
(9) Mathies, R.; Brito Cruz, C. H.; Pollard, T. W.; Shank, C. V. *Science* **1988**, *240*, 777.
(10) Haran, G.; Wynne, K.; Xie, A.; He, Q.; Chance, M.; Hochstrasser, R. M. *Chem. Phys. Lett.* **1996**, *26*, 389.
(11) Ye, T.; Friedman, N.; Gat, Y.; Atkinson, G. H.; Sheves, M.; Ottolenghi, M.; Ruhman, S. *J. Phys. Chem. B* **1996**, *103*, 5122.
(12) Hasson, K. C.; Gai, F.; Anfinrud, P. A. *Proc. Natl. Acad. Sci. U.S.A.* **1996**, *93*, 15124.
(13) Haacke, S.; Vinzani, S.; Schenkl, S.; Chergui, M. *ChemPhysChem.* **2001**, *2*, 310. Haacke, S.; Schenkl, S.; Vinzani, S.; Chergui, M. *Biopolymers* **2002**, *67*, 306.
(14) Du, M.; Fleming, G. R. *Biophys. Chem.* **1993**, *48*, 101. Kennis, J. T. M.; Larsen, D. S.; Ohta, K.; Facciotti, M. T.; Glaeser, R. M.; Fleming, G. R. *J. Phys. Chem. B* **2002**, *106*, 6067.
(15) Govindgee, R.; Balashov, S. P.; Ebrey, T. G. *Biophys. J.* **1990**, *58*, 597.
(16) Tittor, J.; Oesterhelt, D. *FEBS Lett.* **1990**, *263*, 269.

sional reaction coordinate for this process is accordingly the prime goal of its ultrafast investigation.

Resonance Raman (RR) spectroscopy covers the initial stages of excited-state evolution away from the Franck−Condon (FC) region, demonstrating that numerous retinal degrees of freedom are activated by BR photoexcitation aside from double-bond torsion—particularly double-bond stretches.[17−20] Indeed, an ultrafast phase of spectral evolution decaying in ∼200 fs is observed in transient absorption[9,11] and as a rapid Stokes shift in gated spontaneous emission from excited BR.[21] The appearance of equivalent features in experiments with "locked" BR analogues, where torsion around the C_{13}═C_{14} double bond is blocked, indicates that these brief spectral shifts reflect structural evolution along other coordinates.[11] The same experiments prove that the nearly exponential ∼0.5-ps decay of the fluorescent state involves bond twisting around the active double bond, in agreement with other experiments identifying this as the stage of retinal isomerization. Remarkably, the decay to J_{625} is accompanied by almost no spectral evolution in the absorption and emission bands associated with I_{460}. This spectral stagnation was investigated in our laboratory by measuring the efficiency for dumping population out of the fluorescent state using stimulating emission pumping.[22] Results indicated that the band shapes and cross sections for transitions from the fluorescent state are preserved throughout its lifetime and prove I_{460} to be an intermediate along the reactive BR photocycle.

Several scenarios have been proposed to explain the perplexing spectral invariance in BR's fluorescent state as it evolves toward a geometry where ultrafast internal conversion can take place. One invokes a barrier between the FC region and the crossing point to S_0, reflecting inter-twining of nearly degenerate excited states,[12,22] in analogy with the electronic structure of linear polyenes. Another assigns this behavior to flat and featureless potentials involved in excited-state absorption and emission,[19,23] though reconciling this with concurrent crossing to the ground state is challenging. Selecting the correct scenario is hampered by the fact that, while femtosecond pump−probe experiments determine lifetimes for short-lived intermediates, transient changes in broad electronic transitions do not reveal the underlying changes in chemical bonding and molecular geometry.

One way to obtain such information is by augmenting the probing methods with time-resolved vibrational spectroscopies such as Raman or IR. Shifts in band intensities and frequencies of the active excited-state normal vibrations over time can provide the missing structural information. Visible pump−IR probe experiments have confirmed that retinal isomerization in BR takes less than a picosecond, but vibrational spectra of the evolving excited state were not obtained.[24] Spontaneous RR probing is limited in obtaining the same goal by conflicts of simultaneous time and frequency resolution. Femtosecond stimulated Raman spectroscopy was recently introduced, obtaining optimal simultaneous time and frequency resolution by double-pulse probing with a narrow-band pump and an ultrafast, broadband, and red-shifted Raman probe.[25] In the case of BR, however, the intense fluorescence in the probe spectral window obscured excited-state vibrational signals, providing an alternative measure of excited-state dynamics in the form of Raman-induced nonlinear emission.[26] The results were interpreted in terms of rapid structural evolution in the excited state out of the FC region on a time scale of ∼0.25 ps. How this can concur with the conservation of the fluorescence spectrum and cross section is again unclear.

Impulsive vibrational spectroscopy (IVS) is an alternative approach to obtaining excited-state vibrational dynamics in molecular systems.[27] Photoexcitation with a pulse much shorter in duration than nuclear rearrangements promotes population vertically onto the upper surface in the form of a multidimensional vibrational wave packet.[28,29] When the excitation pulse is also significantly shorter than ground-state vibrational periods, it simultaneously induces ground-state vibrational coherence due to resonant impulsive stimulated Raman scattering (RISRS).[30−35] These coherent states induce modulations in probe transmission, providing measures of absolute vibrational phase, dynamics of dephasing, and also instantaneous frequencies. In both cases, the modes activated are those displaced in the transition and can therefore provide information concerning the geometry changes which accompany photon absorption. This method provides a full record of the vibrational decay process in the minimum required observation time.[36] Since impulsive excitation can simultaneously induce coherences in both electronic manifolds, disentangling the modulations induced by both in probe transmission can be challenging.

Low-frequency spectral modulations (∼160 cm^{-1}) observed in I_{460}-stimulated emission following ∼30-fs photoexcitation have been assigned to excited-state coherent torsion.[37] However, coverage of all Raman-active frequencies in retinal requires sub-10-fs time resolution. In a pioneering study based on dye laser technology Shank, Mathies, and co-workers produced imperfectly compressed 12-fs laser pulses and followed dispersed spectral changes in the range 570−660 nm after impulsive BR excitation with the same pulse.[38] On the basis of Fourier analysis and theoretical modeling, the observed long-lived (>50 fs) spectral modulations were assigned exclusively to RISRS-induced motions, providing information equivalent to ground-

(17) Smith, S. O.; Braiman, M. S.; Myers, A. B.; Pardoen, J. A.; Courtin, J. M. L.; Winkel, C.; Lugtenburg, J.; Mathies, R. A. *J. Am. Chem. Soc.* **1987**, *109*, 31.
(18) Myers, A. B.; Harris, R. A.; Mathies, R. A. *J. Chem. Phys.* **1983**, *79*, 60.
(19) Garavelli, M.; Bernardi, F.; Olivucci, M.; Vreven, T.; Klein, S.; Celani, P.; Robb, M. A. *Faraday Discuss.* **1998**, *110*, 51.
(20) Song, L.; El-Sayed, M. A. *J. Am. Chem. Soc.* **1998**, *120*, 8889.
(21) Schmidt, B.; Sobotta, C.; Heinz, B.; Laimgruber, S.; Braun, M.; Gilch, P. *Biochim. Biophys. Acta* **2005**, *1706*, 165.
(22) Ruhman, S.; Hou, B.; Friedman, N.; Ottolenghi, M.; Sheves, M. *J. Am. Chem. Soc.* **2002**, *124*, 8854.
(23) Hayashi, S.; Tajkhorshid, E.; Schulten, K. *Biophys. J.* **2003**, *85*, 1440.
(24) Herbst, J.; Heyne, K.; Diller, R. *Science* **2002**, *297*, 822.
(25) McCamant, D. W.; Kukura, P.; Mathies, R. A. *Appl. Spectrosc.* **2003**, *57*, 1317.
(26) McCamant, D. W.; Kukura, P.; Mathies, R. A. *J. Phys. Chem. B* **2005**, *109*, 10449.
(27) Dhar, L.; Rogers, J. A.; Nelson, K. A. *Chem. Rev.* **1994**, *94*, 157.
(28) Mukamel, S. *Principles of nonlinear optical spectroscopy*; Oxford University Press: New York, 1995.
(29) Zewail, A. H. *J. Phys. Chem. A* **2000**, *104*, 5660.
(30) Chesnoy, J.; Mokhtari, A. *Phys. Rev. A* **1988**, *38*, 3566.
(31) Ruhman, S.; Kosloff, R. *J. Opt. Soc. Am. B* **1990**, *7*, 1748.
(32) Banin, U.; Ruhman, S. *J. Chem. Phys.* **1993**, *98*, 4391.
(33) Ashkenazi, G.; Banin, U.; Bartana, A.; Kosloff, R.; Ruhman, S. *Adv. Chem. Phys.* **1997**, *100*, 229.
(34) Banin, U.; Bartana, A.; Ruhman, S.; Kosloff, R. *J. Chem. Phys.* **1994**, *101*, 8461.
(35) Gershgoren, E.; Vala, J.; Kosloff, R.; Ruhman, S. *J. Phys. Chem. A* **2001**, *105*, 5081.
(36) Banin, U.; Kosloff, R.; Ruhman, S. *Chem. Phys.* **1994**, *183*, 289.
(37) Hou, B.; Friedman, N.; Ottolenghi, M.; Sheves, M.; Ruhman, S. *Chem. Phys. Lett.* **2003**, *381*, 549.
(38) Dexheimer, S. L.; Wang, Q.; Peteanu, L. A.; Pollard, W. T.; Mathies, R. A.; Shank, C. V. *Chem. Phys. Lett.* **1992**, *188*, 61.

state RR spectra.[39] More recently, Kobayashi and co-workers applied ~5-fs non-collinear optical parametric amplifier (NOPA) pulses in the same spectral region to conduct a similar experiment.[40] In contrast to the earlier study, the authors argued that the briefness of the excitation excluded RISRS activity, and a sliding window Fourier transform (SWFT) of the observed modulations was interpreted in terms of an intricate sequence of events taking place exclusively on the excited potential surface, leading from the FC configuration to the isomerized ground state.

The conclusions of the reported IVS studies of BR conflict diametrically. Simulations show that excitation with pulses as short as 1/10 of the ground-state vibrational period can still lead to substantial RISRS contributions to pump−probe signals when the active coordinate is strongly displaced in the transition.[34] Thus, the assumption made by Kobayashi et al. that the use of 5-fs pulses rules out RISRS excitation is unsubstantiated. On the other hand, the initial ~50-fs pump−probe delay was discarded by Pollard and co-workers in the interpretation of the first study,[39] leading to exclusive focusing on the RISRS features. The SWFT analysis reported by Kobayashi shows strong and rapidly damped modulations during the initial 100−200 fs which might correctly be associated with excited-state evolution. As reported from this laboratory, at least in low-frequency modes, excited-state wave packet motions do modulate the spectral signatures of I_{460} for hundreds of femtoseconds,[37] and it is not obvious why coherences in higher frequency displaced modes would not persist as well.

In the present study, we investigate photoexcited dynamics in BR with IVS using transform-limited ~7-fs NOPA pulses. Testing our results with various methods of Fourier analysis, we find that long-lived spectral modulations observed in the dispersed pump−probe signals from BR at wavelengths above 540 nm are dominated by ground-state RISRS signals. Contrary to the unusual wavelength variation of the Raman peak amplitudes reported by Pollard et al., RISRS modulations in our data behave as expected for a molecular chromophore devoid of vibronic structure in absorption due to heavy broadening. Probe wavelengths below 540 nm, tested here for the first time, show new vibrational features which indicate that impulsively excited wave packets persist along bound excited-state coordinates for hundreds of femtoseconds, including brief activity in the frequency range associated with HOOP vibrations. The significance of this finding is discussed in view of recent studies pointing to the involvement of HOOP modes in BR and Rhodopsin isomerization.[41,42]

Experimental Section

Halobacterium salinarum was grown from the S9 strain, and purple membranes containing bacteriorhodopsin were isolated as previously described.[43] Potassium phosphate buffer was used to maintain a neutral pH, and the sample was continuously light adapted by irradiation with IR-filtered light from a 150-W quartz halogen fiber bundle light source. The suspension was circulated through a 250-μm-path length cell equipped with 150-μm quartz windows using peristaltic or bi-directional

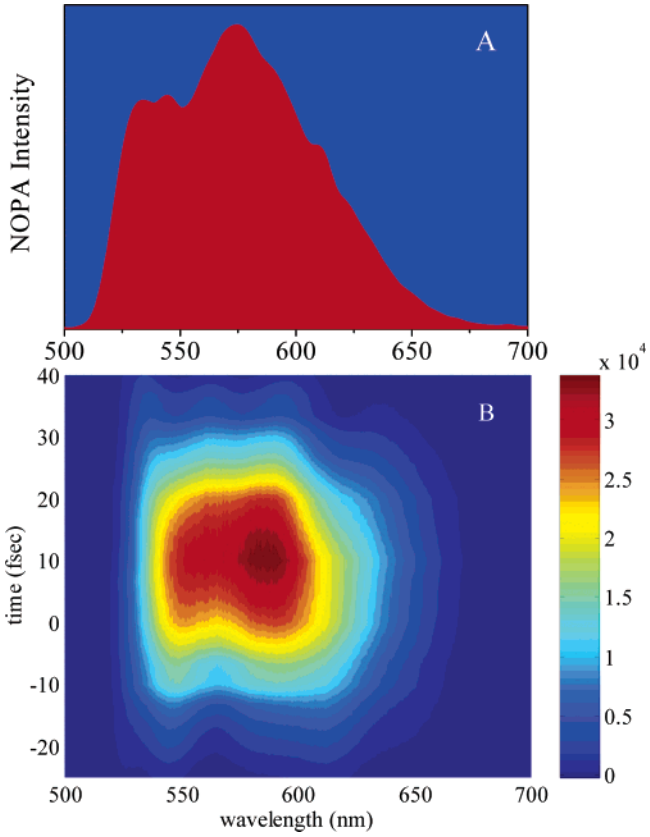

Figure 1. Typical spectrum (A) and frog trace (B) of NOPA pulses used in these experiments. See text for details.

syringe pumps. The optical density of the samples was maintained above 0.25 at 570 nm. The laser system was a home-built multipass amplified titanium−sapphire apparatus, producing a 1-kHz train of 0.5-mJ pulses centered at 800 nm, with temporal and spectral fwhm of 30 fs and 40 nm, respectively. Fifty percent of the amplifier output was used to pump a commercial non-collinear optical parametric amplifier (NOPA plus, Clark-MXR), which was reconfigured to a single pass of amplification in 2 mm of BBO.[44] The NOPA pulses contained 3 μJ of energy, with a spectrum of ~100 nm fwhm centered at 600 nm. To obtain the data over a broad range of probing wavelengths, the central frequency of the NOPA spectrum was tuned to accentuate the blue or red edge of the spectrum. Figure 1 brings a spectrum of the pulses used to obtain probing data below 600 nm, along with a contour plot of the FROG measurement after the pulse compression.

The NOPA output was fed into a zero-dispersion shaper constructed from a 300 l/mm grating, a silver-coated 500-mm focal length spherical reflector, and a 19-channel silver-coated deformable mirror (DM, OKO Flexible Optical) positioned at the Fourier plane.[45] The DM and the grating are vertically and not horizontally displaced to reduce the intrinsic dispersion of the pulse shaper. This setup was capable of completely compressing the NOPA pulses without use of any other means of dispersion pre-compensation, such as chirped mirrors[46] or prism pairs.[47] Compression was conducted by optimizing second harmonic generation (SHG) in a 20-μm BBO crystal. The SHG signal from an amplified photodiode was digitized and used as the pulse fitness in an automated random searching routine. The algorithm used has been

(39) Pollard, W. T.; Dexheimer, S. L.; Wang, Q.; Peteanu, L. A.; Shank, C. V.; Mathies, R. A. *J. Phys. Chem.* **1992**, *96*, 6147.
(40) Kobayashi, T.; Saito, T.; Ohtani, H. *Nature* **2001**, *414*, 531.
(41) Terentis, A. C.; Ujj, L.; Abramczyk, H.; Atkinson, G. H. *Chem. Phys.* **2005**, *313*, 51.
(42) Kukura, P.; McCamant, D. W.; Yoon, S.; Wandschneider, D. B.; Mathies, R. A. *Science* **2005**, *310*, 1006.
(43) Oesterhelt, D.; Stoeckenius, W. *Methods Enzymol.* **1974**, *31*, 667.
(44) Cerullo, G.; De Silvestri, S. *Rev. Sci. Instrum.* **2003**, *74*,1.
(45) Zeek, E.; Maginnis, K.; Backus, S.; Russek, U.; Murnane, M.; Mourou, G. R.; Kapteyn, H.; Vdovin, G. *Opt. Lett.* **1999**, *24*, 493.
(46) Kobayashi, T.; Baltuska A. *Meas. Sci. Technol.* **2002**, *13*, 16. Armstrong M.; Plachta, P.; Ponomarev, E. A.; Ogilvie, J. P.; Nagy, A. M.; Miller, R. J. D. *Appl. Phys. B: Lasers Opt.* **2002**, *74*, S127.
(47) Baum, P.; Lochbrunner, S.; Gallmann, L.; Steinmeyer, G.; Keller, U.; Riedle, E. *Appl. Phys. B* **2002**, *74* [Suppl.], S219.

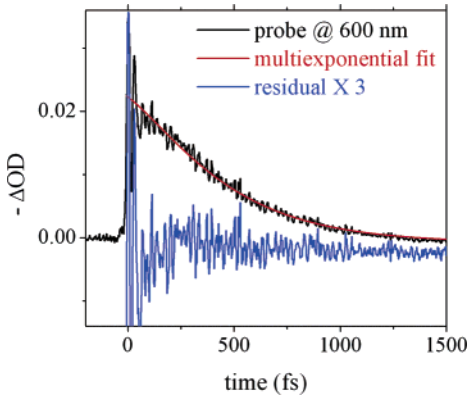

Figure 2. Transient absorption using dispersed probe detection at 600 nm. Isolation of periodical spectral modulations by subtraction of smooth multiexponential fit to the signal decay is demonstrated. The residual used for Fourier analysis is presented on an expanded scale.

described in the literature and is based on random mutations.[48] The total population of a given generation consisted of 45 solutions for voltages on the mirror, 5 of which were parents or best solutions from a previous generation, and 40 offspring generated by their mutation. Optimization was terminated when no further improvement in the fitness was obtained for at least five generations within the experimental noise (~1%). The change in the optimal mirror voltages from the previous generation was another convergence criterion and was required to be below 5 V on all pixels before the termination of an optimization run.

The compressed pulses were characterized in a polarization gate FROG setup, which uses a 0.2-mm fused silica flat as the Kerr medium.[49] A fraction of the amplifier fundamental at 790 nm was used as the gating pulse, providing a transmission gate fwhm of ~25 fs. The gate/NOPA time delay was automatically varied and the gated radiation directed by fiber to a 1/8 meter imaging spectrograph (Oriel) equipped with a CCD camera (Andor Technology). A typical FROG contour plot of compressed NOPA pulses is presented in panel B of Figure 1. In order to verify that optimal compression could be achieved within the deformation limits of the mirror, care was taken that none of the 19 mirror voltages was either saturated or set to zero when the routine converged. As another test, we added 0.5-mm fused silica to the optical beam path. The automated compression routine was run again and the FROG trace compared with that obtained without the extra glass. The results were identical within error, proving that the optimal solution was well within the pulse shaping limits of the apparatus. We note that a slight degree of chromatic separation was observed when the full voltage was applied to all pixels. Nonetheless, the latter test demonstrated that this was not a factor in determining the pulse fitness or the optimal GDD.

The NOPA pulses were split into pump, probe, and reference beams using 0.5-mm fused silica metallic beam splitters which were compensated for in the appropriate beam paths. The former two were focused with reflective optics into the sample at an angle of 3°. Pump pulse energy was 100−150 nJ, and the 1/e intensity diameter of the pump beam was determined by transmission through a pinhole to be 140 μm. The intensities of reference and probe pulses were detected with amplified photodiodes through interference filters which were either 10 or 3 nm in bandwidth. The signals were directly digitized and also recorded differentially in a lock-in amplifier. The variations in transmission were corrected for drifts in the pump and probe intensities, after demonstrating linearity of the signal in both. Positively and negatively chirped pump pulses were obtained by introducing or extracting 0.5 mm of fused silica from the pump beam after compression

(48) Zeek, E.; Bartels, R.; Murnane, M. M.; Kapteyn, H. C.; Backus, S.; Vdovin, G. *Opt. Lett.* **2000**, *25* (8), 587. Bartels, R. A. Ph.D. thesis, University of Michigan, 2002.
(49) Trebino, R.; DeLong, K. W.; Fittinghoff, D. N.; Sweetser, J. N.; Krumbugel, M. A.; Richman, B. A.; Kane, D. J. *Rev. Sci. Instrum.* **1997**, *68* (9), 3277.

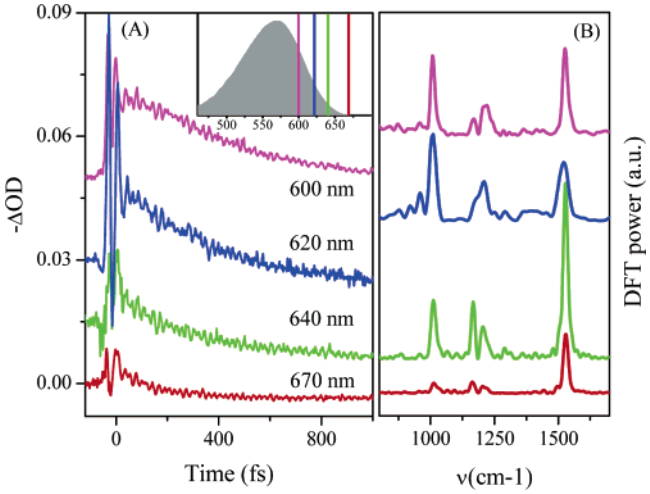

Figure 3. (A) Transient absorption scans following photoexcitation at $t = 0$ with ~7-fs NOPA pulses for a series of dispersed probe wavelengths $\lambda_{probe} \geq 600$ nm. (B) Fourier transform of the spectral modulations after background subtraction from the data in panel A. See text for details.

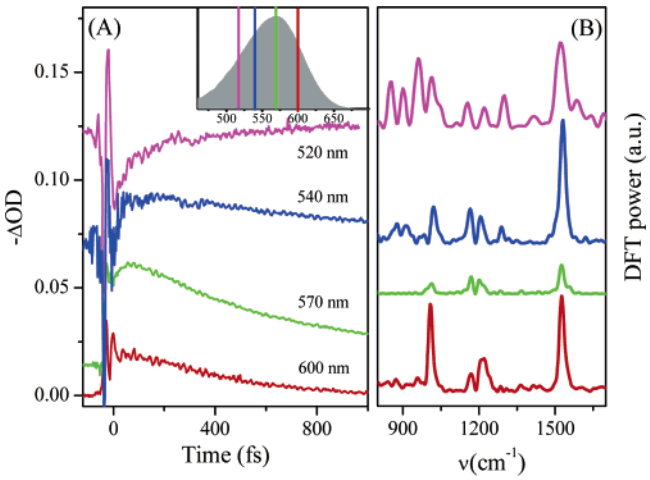

Figure 4. Same as in Figure 3 for $\lambda_{probe} \leq 600$ nm.

of the pulses was complete. With a GVD of 28 fs^2 rad^{-1} and a TOD of only ~12 fs^3 rad^{-2}, the quartz plate introduces almost perfectly linear GDD, broadening the 7-fs fwhm pulses to ~15 fs for both positive and negative chirp.

Results

Probing was conducted from 520 to 670 nm, limited by the spectral range covered by the NOPA. Figure 2 presents typical data for dispersed probe detection through a 10-nm-wide interference filter, in this case centered at 600 nm. At this wavelength, photoexcitation leads to enhanced transmission due to BR ground-state bleaching. High-frequency periodic modulations are discernible on top of the bleach recovery, which are assigned to wave packet motions along bound degrees of freedom in the optically coupled states as discussed above. The oscillatory component is obtained by subtracting a multiexponential fit to the slowly varying background, as demonstrated in Figure 2. Raw data obtained at a series of probing frequencies above and below 600 nm are presented in Figures 3 and 4, respectively. Insets to both figures display the probing wavelength bands in relation to the BR absorption spectrum. At all wavelengths, aside from sharp spikes due to SFM during pump−probe overlap, changes in transmission are observed which

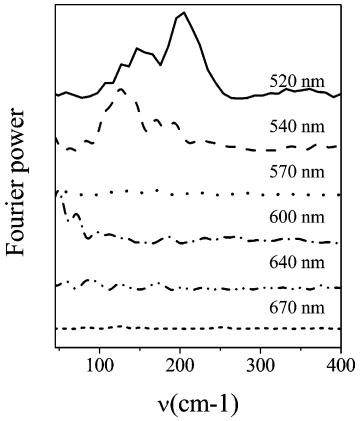

Figure 5. Low-frequency portion (100−400 cm^{-1}) of Fourier transforms presented in Figures 3 and 4.

match the known trends due to the transition from BR_{570} to the fluorescent state followed by decay to the "J" intermediate.[11,12] Superimposed on all of these, one observes the rapid intensity modulations which decay with delay time similarly to the residual displayed in Figure 2.

Power spectra of discrete Fourier transforms (DFT) derived from these modulations after background subtraction and discarding the initial 30−40 fs of pump−probe delay are presented in panels B of Figures 3 and 4 for frequencies above 800 cm^{-1}. DFT spectra at low frequencies are presented for all probe wavelengths in Figure 5. The ordinate of the curves in panels A is absolute ΔOD, and the DFTs are performed without any normalization of the spectral modulations. Figures 3 and 4 demonstrate that the depth of modulation induced by the vibrational coherences depends strongly on the probing wavelength band. In particular, the modulations observed at 570 nm, the ground-state absorption maximum, are obviously shallower than those observed above and below this wavelength.

Four main features show up in the DFTs presented in Figure 3, with the most dominant centered at 1530 and 1008 cm^{-1}. The Fourier analysis reported by Dexheimer and Pollard et al.[38,39] produced equivalent spectral features that were assigned to C═C double bond stretches and methyl rocking motions in the ground state, respectively. Between these lines, a doublet structure of lesser intensity appears which is centered at ∼1170 cm^{-1} and assigned to single C−C bond stretches and CCH rocks. These same features also appear in the Fourier analysis of spectral modulations presented in Figure 4, and their amplitude as a function of probe wavelength is presented in Figure 6, along with $d\alpha/d\nu$ of BR's visible absorption band. The shift in amplitude with probing wavelength differs from line to line, yet for all these features a bi-lobed intensity distribution is apparent with a minimum at 570 nm. When the dispersed probe band is below 570 nm, new lines appear in the DFT, which become stronger the further the spectral observation window is tuned to the blue. These new features consist of a single peak centered at 1290 cm^{-1}, appearing at probe wavelengths of 540 and 520 nm, and broad activity in the 850−950 cm^{-1} range, characteristic of HOOP vibrations which are nearly inactive in the RR spectra of BR.[17,18] We note here that the duration of high-quality data at 620 and 520 nm was limited to 1 ps in pump−probe delay, leading to unphysical broadening of the DFT spectra for these wavelengths.

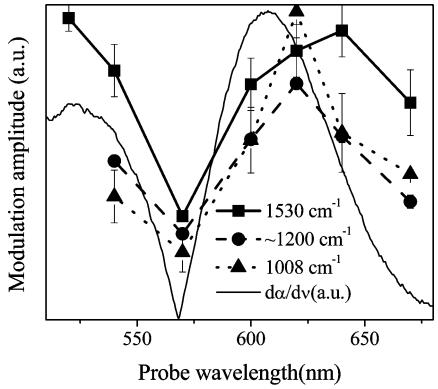

Figure 6. Amplitudes of spectral modulation for four main vibrational features as a function of the dispersed probe wavelength. Included is plot of the first derivative of ground-state bacteriorhodopsin absorption (after subtraction of scattering component) with respect to photon frequency, as a function of photon wavelength.

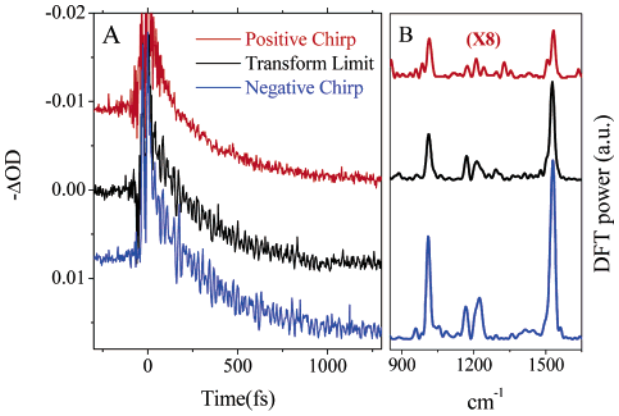

Figure 7. Same as in Figures 3 and 4 for 640-nm probing after excitation with transform-limited, positively chirped, and negatively chirped pump pulses.

Separating the effects of excited- and ground-state wave packets on the transient absorption following impulsive excitation is difficult, and in the particular case of BR it is the subject of debate in the literature. To sort this out, we conducted pump−probe experiments with chirped pump and transform-limited probe pulses. Scans at a probe wavelength of 640 nm for a positive and negative GVD of ∼30 fs^2/rad are compared with the results obtained using a transform-limited pump in Figure 7. Panels A and B show the raw data and the resulting DFT curves, respectively. While the background changes in OD are identical in all three scans, the introduction of this amount of chirp has a profound effect on the amplitude of the observed modulations, causing a doubling of the line intensities in the power spectrum presented in panel B for the case of negative chirp and a reduction by a factor of nearly 8 for a positive chirp of the same magnitude. It is noteworthy that, while these very significant changes take place in the intensity of the spectral modulations, the introduction of chirp into the pumping pulses has nearly no effect on the relative intensities of the four vibrational lines discussed above and appearing in all three spectra.

SWFT analysis was conducted for the isolated modulations obtained from the data presented in Figures 3 and 4 using a supergaussian window of variable width. The resulting spectrograms plot the Fourier amplitude as a function of the position of the windows origin with respect to the zero of pump−probe

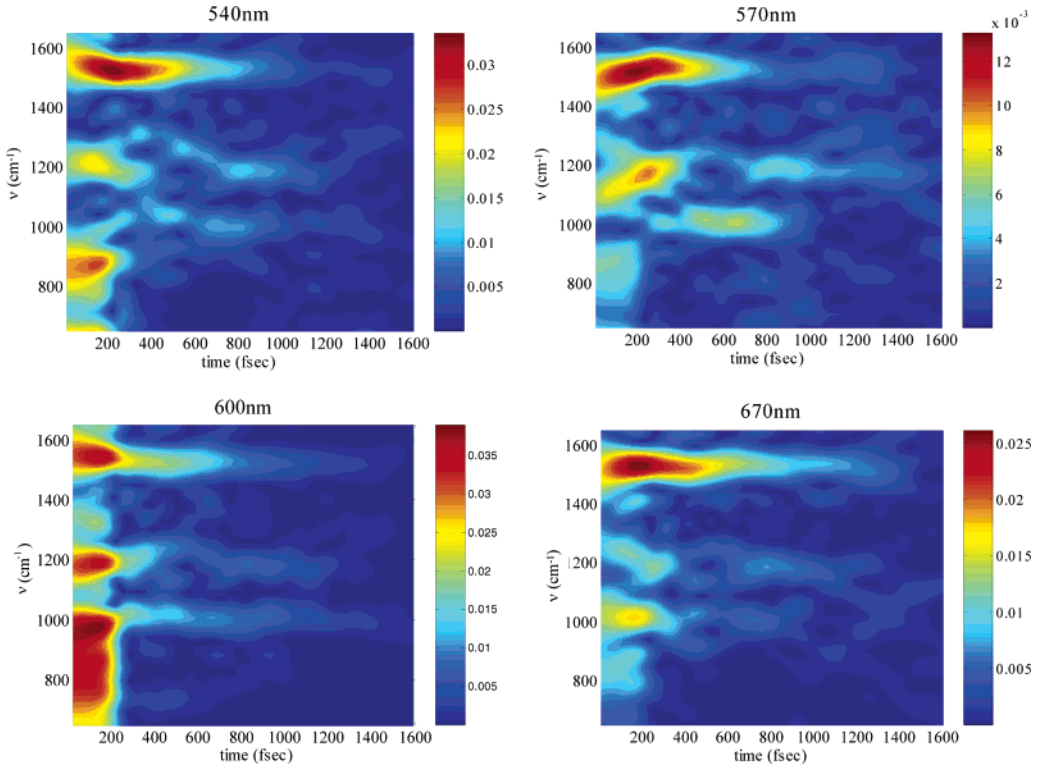

Figure 8. Sliding window Fourier analysis of spectral modulations derived from data at 540, 570, 600, and 670 nm using a supergaussian window of 400 fs in width.

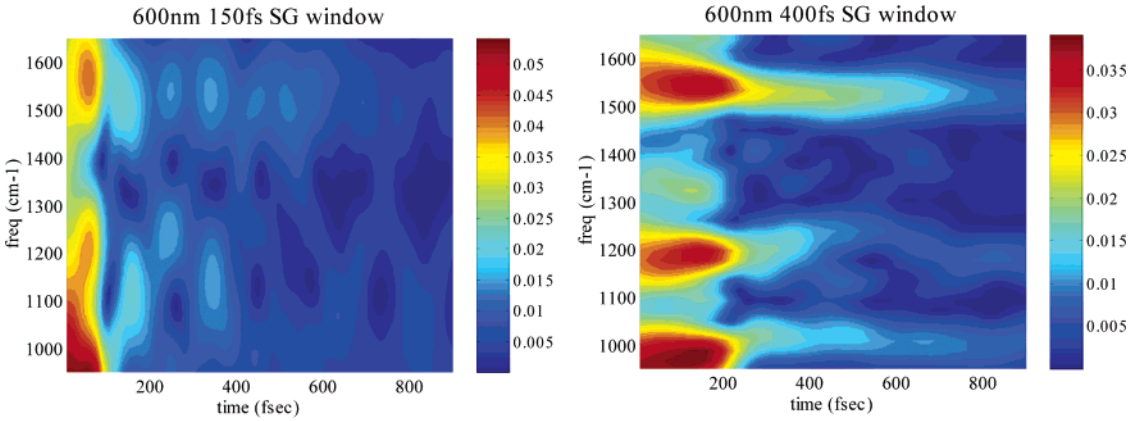

Figure 9. Sliding window Fourier analysis of 600-nm spectral modulations using 400- and 150-fs supergaussian windows.

delay. Figure 8 exhibits spectrograms at four probing frequencies using a window of 400 fs fwhm, which is significantly broader than that employed by Kobayashi et al.[40] Using this window, the three long-lived vibrational features which dominate the DFTs derived from the whole curve are observed at all times beyond the first ~200 fs of delay. In addition, short-lived activity in the HOOP vibrational frequency range is also observed at all probing wavelengths. Even with this broad window, some beating effects are observed in the fingerprint region where the closely spaced doublet is positioned. To determine the effect of window duration on the appearance of the spectrogram, the modulations isolated from the 600 nm probing data were subjected to sliding window Fourier analysis with a shorter window duration of 150 fs, and the results are presented in Figure 9. The results closely resemble those presented in ref 40, including the periodical variations in the apparent frequency shifts in the C═C stretch.

Impulsive vibrational spectroscopy provides information about not only the frequency of nuclear motions but also its phase and rate of decay. In turn, these measures may assist the effort to determine which electronic surface is involved in producing a specific component of the vibronic modulations.[50] Using synthesized data, SWFT analysis, and gradual truncation of the DFT analysis range proved best for determining decay times of individual spectral components. The results for these estimates are condensed in Table 1, along with the measured frequencies of the discernible spectral features extracted from the different dispersed probing scans. The phase of a specific Fourier component of the modulations can be obtained by determining the zero of pump−probe delay with high precision and nonlinear least-squares fitting methods for reconstructing the observed modulations. This was not performed for all of

(50) Carson, E. A.; Diffey, W. M.; Shelly, K. R.; Lampa-Pastirk, S.; Dillman, K. L.; Schleicher, J. M.; Beck, W. F. *J. Phys. Chem. A* **2004**, *108*, 1489.

Table 1. Frequencies, Decay Times, and Absolute Phase of the Main Spectral Modulation Components Derived from Fourier Analysis

ω (cm^{-1})	λ_{probe} (nm)	τ (fs)	ϕ (rad)
1530	520	390 ± 40	−1.5 ± 0.1
	540	500 ± 50	
	570	575 ± 25	
	600	450 ± 50	
	620	450 ± 50	1.6 ± 0.2
	640	650 ± 50	
	670	700 ± 50	
1290	520		
	540	250 ± 50	
1008	520	500 ± 100	0.1 ± 0.1
	540		
	570		
	600	375 ± 25	
	620	600 ± 100	3.0 ± 0.1
	640	700 ± 100	
	670	500 ± 50	
HOOP	520	100 ± 25	
	540	120 ± 25	
210[a]	520	300 ± 25	
135[a]	520	250 ± 25	

[a] Low frequency.

the measurements. Consecutive scans at 620 and 520 nm, to the red and blue of the ground-state absorption peak, were collected with preservation of pump−probe timing, and the resulting modulations were analyzed by nonlinear curve fitting to a superposition of three exponentially decaying harmonic modulations. The phase obtained for the highest frequency component at 1530 cm^{-1} was found to be shifted in phase by 3 rad (±0.2) in the modulations extracted from data at these two frequencies. Thus, the high-frequency modulations which dominate the vibrational response are perfectly anti-phased at these probing frequencies within our experimental error.

Discussion

Our objective was to determine which impulsive spectral features in dispersed BR pump−probe data reflect motions in the reactive excited state, and from their scrutiny to chart the reaction coordinate leading to internal conversion and isomerization. In view of the conflicting conclusions of previous attempts, surmounting the first hurdle is essential. In this respect, the suggestion that a single data set can reproduce the products of both earlier analyses is significant, as it implies that the reported discrepancies stem from different methods of analysis and not from gaps in experimental capabilities. This seems to be the case, as demonstrated in Figures 3, 4, and 9. Accordingly, we approach the question of spectral assignment of the vibrational coherences by reviewing the characteristic signatures of ground- and excited-state vibrational coherences in pump−probe transient spectra.

Decomposition of subpicosecond BR transient absorption spectra shows that excited-state absorptions and stimulated emission cover most of the visible and NIR.[12] Since the S_0-S_1 absorption spectrum covers most of the visible, deep in the latter is the wavelength range where only excited-state transitions are observed, with the added complexity that absorption and stimulated emission from this state overlap there as well. Widom and Champion[51] have shown that impulsive photoexcitation of heavily broadened molecules in solution will induce a periodical modulation of the first moment of the ground-state absorption spectrum due to RISRS coherences, leading to an amplitude of absorption modulation which is maximal on the wings of the absorption band, goes through a minimum near its peak, and reverses phase on either side of the central minimum.[32−34] RISRS activity will extend beyond the range of ground-state absorption, particularly to the red end for high-frequency active modes. The frequency of modulation matches the Bohr frequency defined by the ground-state vibrational energy gaps, with the possible excitation of associated hot bands and harmonics as well. This pattern matches simulations of such an idealized system reported by Pollard et al.,[39] and dye solution experiments conducted by Malkmus et al.,[52] both relating to ultrafast pump−dispersed probe experimental configurations.

The Widom−Champion formalism also allows prediction of the relative amplitudes of modulation due to different active modes.[51] Following notation used in the cited reference, $\bar{P}_g^{(imp)}(t = 0) \propto |\mu|^2 E^2 \omega_0 \Delta$, where $\bar{P}_g^{(imp)}(t = 0)$ represents the initial first moment of the dimensionless momentum along the specified harmonic mode of frequency ω_0 under impulsive excitation conditions, which is displaced upon transition to the upper potential by Δ in reduced coordinate units, and E is the exciting field amplitude. The amplitude of the resulting coherent motion along this coordinate over time is linearly proportional to this momentum kick and is accordingly $\omega_0\Delta$-dependent as well. Since the vertical potential energy difference between the electronic surfaces is $\omega_0\Delta$-dependent, $A(\omega_0,D)$, the resulting amplitude of spectral modulation resulting from the RISRS mechanism involving the specified mode, will be proportional to $(\omega_0\Delta)^2$. A Fourier amplitude spectrum of RISRS modulations in optical density should accordingly resemble the RR spectrum [$\propto(\omega_0\Delta)^2$ for preresonance conditions, or D^2 on resonance]. In a Fourier *power* spectrum of these modulations, the peak intensities are thus expected to exhibit a quartic dependence of the band intensities on ω_0 and on Δ.

As for the effect of chirp on the amplitude of vibronic spectral modulation, it is well established that a correct amount of negative linear chirp can selectively enhance the amplitude and compactness of ground-state vibrational coherences, leading to enhanced amplitude in RISRS spectral modulations.[53,54] A recent study has mapped out the dependence of this effect on the degree of pulse chirping,[52] and this measure has been applied to separating excited- and ground-state wave packet signatures observed in coherent nuclear motion in polydiacetylene chains.[55] This effect is associated with a following of the evolution of the vertical potential energy gap between the optically coupled states by the instantaneous field frequency.[56] A full understanding of this effect is still pending, as the simple models constructed for investigating this theoretically disregard much of the complexity in the large solvated polyatomic molecules often experimented with.

(51) Kumar, A. T. N.; Rosca, F.; Widom, A.; Champion, P. M. *J. Chem. Phys.* **2001**, *114*, 701.
(52) Malkmus, S.; Durr, R.; Sobotta, C.; Pulvermacher, H.; Zinth, W.; Braun, M. *J. Phys. Chem. A* **2005**, *109*, 10488.
(53) Bardeen, C. J.; Wang, Q.; Shank, C. V. *J. Phys. Chem. A* **1998**, *102*, 2759.
(54) Bardeen, C. J.; Wang, Q.; Shank, C. V. *Phys. Rev. Lett.* **1995**, *75*, 3410; *J. Phys. Chem. A* **1998**, *102*, 2759.
(55) Lanzani, G.; Zavelani-Rossi, M.; Cerullo, G.; Comoretto, D.; Dellepiane, G. *Phys. Rev. B* **2004**, *69*, 134302.
(56) Hiller, E. R.; Cina, J. A. *J. Chem. Phys.* **1996**, *105*, 3419.

The characteristics outlined above can assist in assigning the IVS spectral components to ground- and excited-state coherences. Results compiled in Table 1 show that, for probing frequencies above 540 nm, the major spectral features extracted from the total DFT analysis have frequencies which are identical, within experimental error, to bands appearing in RR spectra. The error was estimated by extracting these parameters from multiple data sets. The same features were obtained by Dexheimer et al. in their earlier study which exclusively probed from the peak of BR absorption and to the red.[38] The decay times obtained from SWFT analysis also matches the RR data within our error. The observed spectral lines are significantly enhanced or diminished with the introduction of a moderate amount of negative or positive chirp to the pump pulse, respectively. No new Fourier components were uncovered by the erasure of these prominent bands by the introduction of positive chirp in the pump pulses. Finally, the changes in amplitude and phase of the spectral modulations with shifts in the dispersed probe wavelength match the expected behavior for impulsively induced ground-state wave packets in dispersed pump−probe spectra, including the reversal of phase. Thus, the characteristics outlined above concerning the 1008, 1530, and ~1200 cm^{-1} doublet features in the $\lambda > 540$ nm data all match the earlier assignment of Shank and Mathies and co-workers as hallmarks of RISRS induced ground-state vibrational coherences, not reflecting excited-state evolution.

The relative amplitudes of these features in a single DFT spectrum are, however, perplexing. The discussion above leads to an expectation that the DFT power spectra should exhibit larger differences in intensities (peak areas) of the different bands than observed in the RR spectra for the same modes. Many of the simplifying assumptions which led to the estimated Δ and ω dependence of these measures are not altogether justified—the spectral width is not far greater than the vibrational frequencies, and accordingly the probe wavelength dependence of the modulation depth varies from line to line, exhibiting prominence for the high-frequency feature when probing far from the ground-state electronic absorption peak. Nonetheless, when probing at the half-intensity point of the ground-state absorption band, the intensities of the 1008 and 1530 cm^{-1} lines are nearly equal—far from the 1:5 ratio observed in RR, or the predicted 1:25.

To factor in the effect of finite pulse durations, we estimate the pump−probe cross-correlation from autocorrelation measurements of the laser pulses and compare it with the theoretical transform-limited duration obtained from the spectrum. The latter is near 5 fs, while our non-collinear autocorrelation measurements indicate a pulse width of ~7 fs. Taking the larger of these measures, a cross-correlation of ~11 fs fwhm is obtained. Convolution of the spectrum with the matching frequency response leads to an intensity factor of no more than 0.6 between the peaks at 1530 and 1008 cm^{-1}. Any overestimation of the pulse cross-correlation will only reduce this factor. Even if this is squared for comparison with power spectra, it only makes for a correction factor of ~2.5. Furthermore, the insensitivity of the DFT spectrum to positive and negative chirping of the pump, as shown in Figure 7, suggests that the experimental cross-correlation is actually significantly shorter than estimated from the autocorrelation measurements, leaving the discrepancy of the relative band intensities an open question.

While the frequencies of the dominant features observed in the full DFT for $\lambda_{probe} \geq 570$ nm match the results reported by Dexheimer and Pollard et al., the absolute depth of spectral modulation and the relative intensities of these features in any given spectrum do not. In particular, while the weakest modulations appear in our data when probing at 570 nm, Dexheimer, Pollard, and colleagues reported a maximal depth of modulation at this wavelength (568 nm). Instead of the regular variation of line intensity with probe wavelength demonstrated in Figure 6, the earlier study reported irregular shifts from one probe wavelength to the next. Through simulation, these trends were attributed to the finite duration of the probe pulses, leading to large variations of field intensity within the BR absorption band. Since the pulse spectrum used here is only moderately broader than that employed by Dexheimer et al., this effect must not be the whole story.

As shown in Figure 4, when the dispersed probe is recorded at 540 and 520 nm, new spectral features show up in the DFT. These consist of a line centered at 1290 wavenumbers, a clump in the 850−1000 cm^{-1} range, and an equally broad and intense feature in the torsional frequency range from 100 to 250 cm^{-1}. In addition to these new lines, high- and low-frequency shoulders grow in to the 1008 and 1530 cm^{-1} lines, respectively. It is known that 540 nm marks the red edge of an abrupt rise in BR excited-state absorption, and it is thus probable that the oscillatory modulation features which grow in below this wavelength are due to that absorption and reflect excited-state vibrational coherences. The estimated decay times seem to be in accord with this assignment as well, since they are consistently shorter than the lifetimes of the features assigned to RISRS but are too long to be assigned to background subtraction artifacts. Their similarity at the two bluest probing frequencies bolsters this assertion. The only exception in this respect is the 1290 cm^{-1} band, which decays at a rate on par with that observed in the RISRS features.

This assignment poses new riddles concerning the generation mechanisms of the observed wave packets. Intense excited-state wave packets are generated along coordinates which are strongly displaced with respect to the ground state. The activity thus generated may not lead to appreciable modulations in absorption to an even higher excited electronic state unless the same condition is met, i.e., that a significant displacement along this coordinate exists between these two excited states as well. The appearance of strong modulations in excited-state absorption does imply displacements in both transitions (vide supra). It thus follows that these modulations must be associated with bound coordinates having strong Δ values obtained from visible RR studies of BR—the very modes shown to be RISRS active for $\lambda_{probe} > 540$ nm!

Bound-to-bound transitions in large conjugated polyatomic hydrocarbons usually lead to mild shifts in normal-mode frequencies. Picosecond time-resolved RR experiments suggest that the intensely active C=C stretching mode appearing at 1529 cm^{-1} shifts in the excited state to 1580 cm^{-1}.[20] This relatively large increase matches expectations based on ground-state frequency lowering of this mode due to vibronic state mixing.[57] In our data there is no sign of an increase in this frequency in the total DFTs—if anything, the low-frequency shoulder observed might be the signature of a mild reduction in the

(57) Orlandi, G.; Zerbetto, F.; Zgierski, M. *Chem. Rev.* **1991**, *91*, 867.

frequency of the carbon−carbon double-bond stretching modes in the excited state, and the high-energy shoulder in the methyl rock may likewise be due to a stiffening of this mode on the upper surface. The increase in the amplitude of these lines upon tuning the probe to the blue can be understood in terms of the probe frequency dependence exhibited in Figure 6, and need not involve specific contributions from excited-state wave packets. The 1290 cm^{-1} feature could be associated with either the 1220 or 1170 cm^{-1} RR bands, although this would reflect a relatively large shift in vibrational frequency as well.

The most unusual features in the modulation frequency spectrum involve the activity near 900 cm^{-1}. Assuming involvement of modes with similar frequency in the ground state, this would represent short-lived coherent HOOP vibrations in the excited state. But this seems unlikely since the HOOP modes are only marginally active in RR and therefore are not expected to be IVS active in either the ground or excited states. Intriguingly, HOOP mode activity has recently been implicated in the isomerization reaction of the related rhodopsin protein on the basis of femtosecond broadband RR pump−probe experiments reported by the Mathies group.[42] Intense activity in this frequency range was also detected in broadband coherent anti-Stokes Raman spectroscopy (CARS) experiments reported by Atkinson and co-workers for the "J" intermediate in the BR photocycle.[41] Kukura et al.[42] assigned ultrafast HOOP mode activation in rhodopsin to incoherent intramolecular vibrational relaxation, which would not lead to coherent vibrational motion, and accordingly would not give rise to modulations such as those observed in our experiments. Further work, including isotopic labeling and investigations with locked chromophores, will be required to fully assign the underlying modes and the mechanisms of their coherent activation.

This interpretation raises the question of how these motions leave no mark on pump−probe data at longer wavelengths throughout the visible. Aside from the absorption band peaking at 460 nm, excited BR also absorbs intensely in a band peaking at 730 nm, the wing of which extends well into the ground-state absorption range. The same is true of the excited-state emission band, which overlaps with the 730 nm absorption. Accordingly, the fact that no matching modulations were detected even at 670 nm is puzzling. The absence of modulations in the 730 nm excited-state absorption might be assigned to unfavorable geometrical changes with respect to the reactive excited state. Fluorescence, however, takes place between the same states responsible for RISRS generation—and must register the induced vibrations as pronounced spectral modulations in stimulated emission for the highly displaced modes. It is possible that excited-state coherences produce more intense modulations in the 460 nm absorption band because of the steep rise in OD near 520 nm.

The main supporting evidence in terms of IVS that the fluorescence and "blue" absorption bands originate from the same excited state comes from observations of low-frequency modulations (100−200 cm^{-1}) in stimulated emission in the NIR which roughly match those depicted in Figure 5.[37] It is important to address this, since recent studies have even assigned the subpicosecond emission band in BR to nonreactive population unrelated with the photocycle.[58] Truncated data set analysis reveals that the apparent frequency of the torsional feature

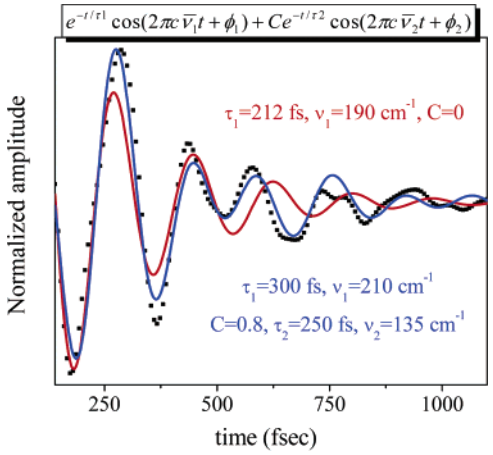

Figure 10. Curve-fitting analysis to the low-frequency modulations detected in the 520-nm data. The functional form used is shown, with the important resulting parameters from one- and two-mode fitting.

extracted from 520 nm data evolves with time. To analyze these observations, this portion of the modulation was separated via bandpass filtering and fit to two models—a single damped oscillation and a superposition of two. Results are presented in Figure 10 and in Table 1. The double-mode analysis generates a better but still partial fit to the data, with frequencies of 135 and 210 cm^{-1}, decay times 200−300 fs, and nearly equal amplitudes. The single-mode analysis produces a central frequency of 188 cm^{-1}, very near that reported for 800 nm probing.[37]

Identifying torsional motions which are activated optically, and accordingly functional in photochemistry of retinal proteins, has been the subject of recent experiment and theory.[59,60] Multiple low-frequency features have been identified both in RR and in theory relating to the reactive excited state, but direct comparison of frequencies is complicated by the fact that they relate to different electronic surfaces. The low-frequency activity observed in NIR probing of BR, and that in the emission band of RPSB in solution, were both well fit to the fundamental and first harmonic of a single damped mode. In view of the superior two-mode fit demonstrated in Figure 10, verifying that the modulations observed in both cases reflect the same excited-state motions will require more study. It is in agreement with refs 59 and 60 that multiple torsional modes are active below 300 cm^{-1} in the reactive excited state. The prominensce of the ∼170 cm^{-1} band both in BR and in RPSB in solution would suggest it reflects the symmetric in-plane motion described in both studies, as it seems not to depend on active-site structural "priming" described in both references. These modes are sufficiently low in frequency, however, that even rapid IC could excite them "impulsively" as oulined in ref 51, unlike the HOOP modes discussed above.

Reviewing the preceding discussion in light of the objectives stated at its outset, it seems that advances have been made in identifying excited-state IVS signatures. Using this information to deduce a comprehensive model for photoinduced chemical dynamics still awaits us and will require full coverage of the excited-state absorption with similar time resolution. In this

(58) Abramczyk, H. *J. Chem. Phys.* **2004**, *120*, 11120.
(59) Cembran, A.; Bernardi, F.; Olivucci, M.; Garavelli, M. *J. Am. Chem. Soc.* **2003**, *125*, 12509.
(60) Lin, S. W.; Groesbeek, M.; van der Hoef, I.; Verdegem, P.; Lugtenburg, J.; Mathies, R. A. *J. Phys. Chem. B* **1998**, *102*, 2787.

respect, if and when possible, extending probing to the near-UV might prove beneficial, as pointed out in a recent study with much longer pulses.[61] Results presented here demonstrate that care must be taken when choosing the tools for extracting the dynamic information from IVS. Sliding window Fourier methods are ambiguous due to conflicts of time and frequency resolution, as demonstrated in Figure 9. LPSVD[62] and filter diagonalization[35,63] suffer from the assumption of exponential amplitude variations as well. Thus, all of these options will have to be explored in order to extract the dynamical information available in the excited-state IVS.

Conclusions

Degenerate pump−probe experiments with broadband NOPA pulses were conducted to record the impulsive vibrational spectroscopy of native bacteriorhodopsin at dispersed probing wavelengths from 520 to 670 nm. Sliding window and full-range Fourier analysis of the resulting spectral modulations demonstrates that transient transmission at dispersed probe wavelengths $\lambda_{probe} \geq 570$ nm are predominantly influenced by RISRS-induced ground-state vibrational coherences. This conclusion is based upon the frequencies of spectral modulations, their decay rates, and the variation in their amplitudes with shifts in the dispersed probing wavelength. This was verified by testing the effect of positive and negative linear chirp in the pump pulse on the amplitudes and spectra of the observed modulations. At probing wavelengths of 540 and 520 nm, new vibrational features were observed consisting of high- and low-frequency shoulders adjacent to the strong C═C stretching and methyl rock modes, respectively, which have ground-state frequencies of 1008 and 1530 cm^{-1}, a strong mode at 1290 cm^{-1}, and brief activity centered at ~900 cm^{-1} which is characteristic of ground-state HOOP vibrational modes. Along with the variations at the high-frequency end, activity below 200 cm^{-1} also appears only in this range. Since 540 nm is the red edge of an intense absorption band assigned to the reactive excited state, these new features are tentatively assigned to wave packet motions along excited-state displaced normal vibrational coordinates. While the shoulders may reflect mild frequency variations of the active vibrations in the excited state, the HOOP mode activity is not easily explained in view of the inactivity of these modes in the resonance Raman spectrum. It is particularly intriguing since motions along these coordinates have been implicated in the internal conversion reaction coordinates of rhodopsin and also of BR. Understanding the mechanism of coherence generation in these modes, their assignment to specific coordinates, and an explanation of the absence of their signature and that of the torsional modes in the pump−probe spectral modulations measured at longer wavelengths will require further study.

Acknowledgment. We thank Prof. G. Cerullo, Prof. R. Kosloff, and Dr. C. Manzoni for helpful discussions and O. Bismuth, O. Shoshana, and E. Mastov for technical assistance. This work was supported by the Israel Science Foundation (ISF), which is administered by the Israel Academy of Sciences and the Humanities, and by a grant from the A.M.N. Fund for the promotion of science, culture, and arts in Israel. The Farkas Center is supported by the Minerva Gesellschaft, GmbH, Munich, Germany. M.S. holds the Katzir-Makineni chair in chemistry.

JA064910D

(61) Schenkl, S.; van Mourik, F.; Friedman, N.; Sheves, M.; Schlesinger, R.; Haacke, S.; Chergui, M. *Proc. Natl. Acad. Sci. U.S.A.* **2006**, *103*, 4101.
(62) Wise, F. W.; Rosker, M. J.; Milhauser, G. L.; Tang, C. L. *IEEE J. Quantum Electron.* **1987**, *QE23*, 1116.
(63) Wall, M. R.; Neuhauser, D. *J. Chem. Phys.* **1995**, *102*, 8011. Pang, J. W.; Mandelshtam, V. A. *J. Chem. Phys.* **1998**, *108*, 9999.